Failure of Partially Saturated Frozen Soils: A Micromechanical Analysis

Mehdi Pouragha & Mohammadreza Jebeli
Department of Civil & Environmental Engineering – Carleton University, Ottawa, ON, Canada
Rachel Glade
Department of Earth and Environmental Sciences– University of Rochester, Rochester, NY, United States

ABSTRACT
A micromechanically based failure criterion is developed for shear strength of partially saturated frozen soil. Following a multiscale framework, a relation between the macroscopic stresses and the interparticle forces is formulated, which eventually leads to a failure criterion at the macroscopic level in terms of parameters such as ice strength, matric suction, void ratio, average particle size, and contact fabric. The strength predictions are compared to three different experimental datasets where the model demonstrates good accuracy without resorting to any retrospective calibration. Crucially, the failure model establishes a connection between strength of soil at frozen and unfrozen states, which can be used in estimating the strength degradation in frozen soils upon thawing.

RÉSUMÉ
Un critère de rupture basé sur la micromécanique est développé pour la résistance au cisaillement d'un sol gelé partiellement saturé. Suivant un cadre multi-échelle, une relation entre les contraintes macroscopiques et les forces interparticulaires est formulée, ce qui conduit finalement à un critère de rupture au niveau macroscopique en termes de paramètres tels que la résistance de la glace, la succion matricielle, l'indice des vides, la taille moyenne des particules et la distribution des contacts. Les prédictions de résistance sont comparées à trois ensembles de données expérimentales différentes où le modèle démontre une bonne précision sans recourir à un étalonnage rétrospectif. Fondamentalement, le modèle de défaillance établit un lien entre la résistance du sol à l'état gelé et non gelé, qui peut être utilisé pour estimer la dégradation de la résistance dans les sols gelés lors du dégel.

1   INTRODUCTION

The warming climate in the Arctic regions poses important questions to the safety and performance of the geo-infrastructure in the Northern regions, as well as the environmental issues pertaining to degradation of strength in the frozen soils.

Seminal previous works explored some of the most relevant factors affecting the strength of frozen soils (Chamberlain et al. 1972, Ladanyi 1972, Morgenstern and Anderson 1973, Konrad 1989, Arenson and Springman 2005),   However, The previous literature has focused mainly on ice-rich soils where the mechanical properties can be represented by straightforward averaged values based on the mixture theory formulation. Therefore, the behaviour of partially saturated frozen soils have remained less explored (Liu et al. 2020). The few studies on the topic suggest a non-monotonic variation of frozen soil strength with saturation (Baker 1979, Aksenov et al. 2018). Curiously, the variation resembles the effect of saturation in unfrozen soils where decreasing the water saturation below a certain limit leads to the so-called pendular regime where, at the particle-scale, air, water, and grain phases interact in the form of distinct capillary bridges (Lu and Likos 2004, Pouragha et al. 2018).

Based on the analogy between the frozen and unfrozen states, a change in interaction regimes towards more distinct ice bridges can also be considered for frozen soils at lower saturations, especially for sandy and silty soils as shown schematically in Figure 1. Similar to the unfrozen state, the discrete ice bonds are expected to affect the strength of the frozen media at low saturation. While the micromechanics of saturated frozen soils has been studied in a few recent works (Wang et al. 2020, 2021), the micromechanics of partially saturated frozen soils remains, for the most part, unexplored.
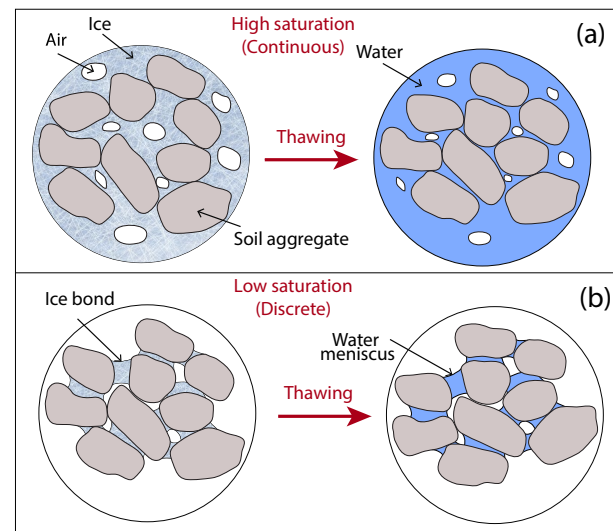

Figure 1. Microstructure of partially saturated frozen and unfrozen soils at (a) high saturations, and (b) low saturations.

In this study, we develop a micromechanical formulation for the strength of frozen silty/sandy soils at relatively low ice saturations. Using multiscale techniques, the strength at the macroscopic scale is related to the cohesive strength of ice bonds, leading to a Mohr-Coulomb-like failure criterion that naturally captures the effect of parameters such as ice content, particle size distribution, void ratio, and temperature. The model predictions have been validated against three different sets of experiments. The model enables us to provide a direct comparison between the shear strength of partially saturated soils at frozen and unfrozen states, estimating the strength degradation in unsaturated soils upon thawing.

2 MICROMECHANICAL FORMULATION

The discrete nature of soil-ice interaction at low saturations (Figure 1-(b)), suggests that the strength of such frozen soils is primarily governed by the cohesive ice bonds. Therefore, we adopt here a micromechancial approach to upscale the strength of bonds and arrive at a global failure criterion at the macroscopic scale.

The formulation procedure is as follows. Assuming spherical particles for simplicity, Young-Laplace equation can be used for the unfrozen state to calculate the geometry of pendular liquid bridges at a given matric suction (Lu and Likos 2004, Wan et al. 2014). When these liquid bridges freeze, the bond geometry is updated to reflect the expansion of ice. The intrinsic strength of ice can then be used to derive a failure via a simple localization/homogenization scheme following the scheme explained in Pouragha et al. (2020). Our calculation procedure adopts the following simplifying assumptions. Particles are spherical; stress and suction are homogeneous; ice bridges exist at all the contact points, and only at contact points; the geometry of an ice bridge is proportional to its associated liquid bridge at unfrozen state; the shear strength of ice follows a Mohr-Coulomb criterion; the failure of ice bonds is assumed to occur along their local tangential direction. Moreover, only fully frozen and fully unfrozen states are considered and therefore, potential effects of thin films of unfrozen water at sub-zero temperatures are not captured.

2.1 Properties and Geometry of Ice Bridges

The shear strength of ice is often expressed using Mohr-Coulomb failure criterion with both cohesion and friction parameters. For the current study, we adopt the ice strength values reported by Fish et al. (1997). The experiments are carried out using triaxial tests capturing also the dependencies on temperatures in the range of 0 to -40°. Values of friction angles between 2°-14°, and cohesion between 5.4-12.90 MPa are reported with the higher values corresponding to lower temperatures. Herein, the rate-dependency of the ice strength has been ignored for the sake of simplicity, noting that extending the formulation to consider rate effects is straightforward. A common value of 9% is also adopted for volume expansion upon freezing ice.

The geometry of ice bridges can be related to those of the capillary bridge before freezing. The imaging results in Huang & Zhou (2020) indicate that the geometry of the eventual ice bridge resembles that of the unfrozen capillary meniscus, see Figure 2. Herein, the geometry of ice bridges is found by applying a 9% homogeneous volumetric expansion to the capillary bridge. The geometry of the capillary bridge is in turn found using Young-Laplace equation and adopting the toroidal approximation suggested by Lu & Likos (2004) as shown in Figure 3.
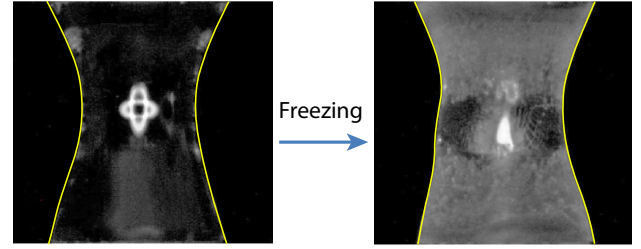

Figure 2. Imaging of freezing process of a capillary bridge (Modified after Huang & Zhou (2020)); (left) unfrozen state, (right) frozen state.
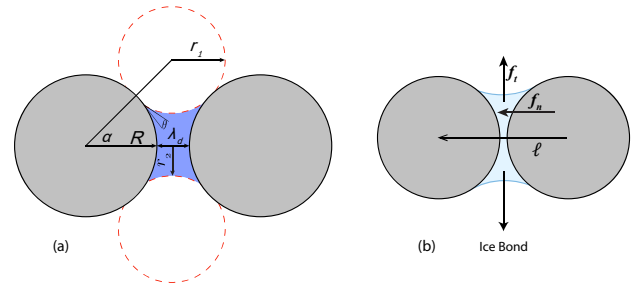

Figure 3. (a) The geometry of the assumed toroid shape given by r_1 and r_2. (b) Schematics of the branch vector and normal and tangential contact forces acting on an ice bridge.

Among others, the radius of the narrowest cross-section of the bridge (neck), r_2, and the volume of the liquid bridge, V_b, are crucial to our calculation, which can be expressed as:

$$r_2 = R\tan\alpha - r_1\left(1 - \frac{\sin\theta}{\cos\alpha}\right),$$
$$V_b = 2\pi R^3 \sin^2\alpha - 2\pi R^3 \sin^2\alpha \cos\alpha - \frac{2\pi}{3}R^3(1 - \cos\alpha)^2(2 + \cos\alpha) - V_r,$$

$$V_r = \pi r_1^2(\pi - 2(\alpha + \theta) - \sin(\alpha + \theta))$$
$$\left(r_1 + r_2 - \frac{(2/3)\,r_1\cos^3(\alpha + \theta)}{(\pi/2) - (\alpha + \theta) - \sin(\alpha + \theta)\cos(\alpha + \theta)}\right) \quad [1]$$

where θ is the contact angles, R is the radius of the particle, r_1 denotes the outer curvature of the bridge, and α denotes the filling angle that depends on the matric suction, $u_a - u_w$, and the surface tension of the interface, T_s, through the Young-Laplace relation $u_a - u_w = T_s(1/r_1 - 1/r_2)$.

For a given value of suction and particle size, the volume of the liquid bridge, V_b, can be calculated. This volume is increased by 9% upon freezing to get the volume of the corresponding ice bridge. Assume the expansion upon freezing to be homogeneous, the updated ice volume is entered into Eq. 1 again to numerically solve for the value of r_2 for the ice bridge.

2.2 Multiscale Failure Criterion

The micromechanical formulation developed in Pouragha et al. (2020) can be adopted here to express the overall strength of the frozen soils in terms of the ice bond strength. The procedure assumes a linear localization relation for contact forces based on homogeneous stress assumption such that the force at any given contact, c, is expressed as

$$f_i^c = B_{ij} n_j^c \qquad [2]$$

with $\boldsymbol{n}$ being the contact unit normal vector. The Love-Weber relation can now be used to calculate the tensor $\boldsymbol{B}$ for spherical particles:

$$\sigma_{ij} = \frac{1}{V} \sum_{\text{all contacts}} f_i^c \ell_j^c \rightarrow B_{ij} = \frac{V}{\bar{\ell} N_c} \sigma_{ik} F_{kj}^{-1} \qquad [3]$$

with V being the volume of the domain, N_c total number of contacts, $\bar{\ell}$ the average branch vector length, $\boldsymbol{\sigma}$ the Cauchy stress tensor, and $F_{ij} = (\sum f_i^c \ell_j^c)/N_c$ is the contact fabric tensor. Further simplification can be made by assuming a homogeneous void ratio, e, such that:

$$\frac{V}{N_c} \simeq \frac{8}{3z}(1+e)\pi R^3 \qquad [4]$$

where coordination number, z, is the average number of contacts per particle. More detail can be found in Pouragha et al. (2020).

The strength of ice bonds at the particle scale is assumed to be given by a threshold on their tangential force component:

$$|f_t| = |f_i t_i| \leq b_{ice} f_n + c_{ice} (\pi r_2^2) \qquad [5]$$

with f_t and f_n are the tangential and normal components of contact force, t_i is the unit vector along the tangential component of f_i, b_{ice} and c_{ice} are the intrinsic friction and cohesion of ice, and the term πr_2^2 is the area of the neck. Recalling that $f_n = f_i n_i$, Eqs. 2-5 can be combined to arrive at the following failure criterion at macroscopic scale.

$$\left| \sigma_{ik} F_{kj}^{-1} t_i n_j \right| - b_{ice}\left(\sigma_{ik} F_{kj}^{-1} n_i n_j\right) - \frac{3z\, c_{ice}\,(\pi r_2^2)}{4\pi R^2(1+e)} \leq 0 \qquad [6]$$

Equation 6 is represents an anisotropic Mohr-Coulomb failure criterion which can be numerically solved for a given value of fabric $\boldsymbol{F}$ to find the failure stresses (Pouragha et al. 2019). For the simpler case of isotropic materials with $F_{ij} = \delta_{ij}/3$, the common Mohr-Coulomb criterion is recovered such that:

$$|\tau| - \tan\varphi\,(\sigma_n) - c \leq 0,$$

$$\tan\varphi = b_{ice}, \qquad c = \kappa_c c_{ice}, \qquad \kappa_c = \frac{z r_2^2}{4R^2(1+e)} \qquad [7]$$

We note that while the friction of the frozen soil is found to be the same as the intrinsic friction of ice, the cohesion is different and depends heavily on geometry of the bonds, as expressed through the coefficient κ_c. For the rest of this study, we consider the isotropic version of the failure function in Eq. 7.

3 PARAMETRIC STUDY

Among the advantages of such micromechanical models is their ability to capture the effect of various material parameters. In this case, the failure criterion in Eq. 7 captures directly the effect of average grain size and void. Other dependencies on temperature, strain rate, and matric suction at the unfrozen state are also taken into account indirectly through their effect on the strength and geometry of the ice bonds. Herein, we present a parametric study to demonstrate the dependency of shear strength of frozen soils on these parameters. The following typical values are chosen as reference for demonstration purposes: $\bar{R} = 0.143\ mm$, $\theta = 0$, $z = 6.0$, $e = 0.7$, $(u_a - u_w) = 16\ kPa$. The average particle size represents Ottawa sand. Also, the ice strength at $-6°C$ reported by Fish et al. (1997) is used.
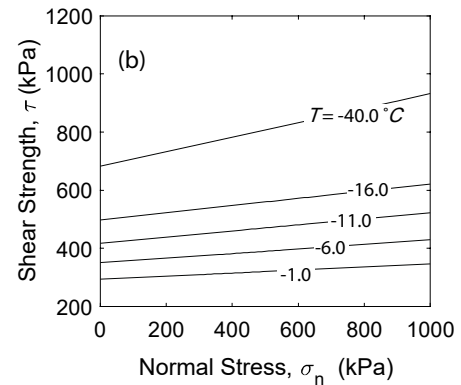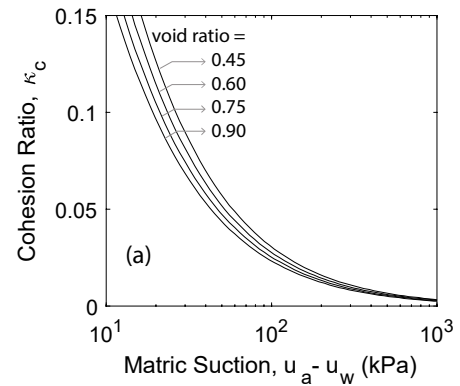

(a)

(b)

Figure 4. (a) Effect of matric suction at the unfrozen state on cohesion of frozen soil. (b) Effect of temperature on the failure envelope of frozen soils.

Figure 4 shows the effect of matric suction, void ratio, and temperature on the shear strength of frozen soils. Note that the matric suction here refers to the matric suction at the unfrozen state corresponding to each particular frozen state. For unfrozen soils, higher matric suctions result in lower saturations and thinner bridges, which, after freezing, yields a smaller value of neck radius, r_2. Thus, an increase in the matric suction is expected to decrease the cohesion of the frozen soils, as verified in Figure 4-(a). Expectedly, frozen soils with higher void ratios are predicted to have lower shear strengths as well.

The temperature effect is visualized in Figure 4-(b) where both cohesion and friction of the frozen soil is predicted to increase for colder temperatures. This is consistent with previous experimental observations (Bragg and Andersland 1981, Bourbonnais and Ladanyi 1985, Yamamoto and Springman 2014).

4 VERIFICATION

The predictions of the failure criterion in Eq. 7 is compared here to two experimental datasets: the shear box experiments of Kim et al. (Kim et al. 2018), and the uniaxial experiments by Cai et al. (Cai et al. 2014). The calculation of strength from Eq. 7 is predicated upon the geometry of the water and ice bridges, which in turn, requires an estimate of suction-saturation relation at the unfrozen state. Herein, we use the formulation presented by Pouragha et al. (2021) where the water retention curve (WRC) is calculated in terms of particle size distribution and void ratio. Moreover, a typical value of $z = 6$ is used for all cases.

It is crucial to note that the verification presented here does not require any retrospective calibration of the model since all the parameters in Eq. 7 can be calculated from the intrinsic properties of ice and other basic information such as particle size distribution.

Figure 5 compares the model predictions with the shear strength reported by Kim et al. (2018) for different silt fractions at saturation of $S_r = 15\%$. The fraction of silt affects the average particle size as well as the WRC, and hence the geometry of the bonds. The sensitivity of the model to the error in suction-saturation relation is visualized by providing the variation interval for $\pm 5\%$ change in saturation. The comparison in Figure 5 shows that not only the model is capable of predicting the shear strength of such frozen soils, it also successfully captures the effect of fine content on the shear strength.

The second experimental dataset used to verify the performance of the proposed failure criterion is from Cai et al. (2014) who performed uniaxial compression tests on frozen sands with saline ice containing 2% of salt. The saturation varied between 45% and 75%. The effect of salinity is readily captured in the failure criterion of Eq. 7 through its effect on the intrinsic strength of ice. In this case, we use the measurements by Smith & Schulson (1994) who performed triaxial tests on saline ice at similar temperatures. Figure 6 shows the comparison between the model predictions and the experimental measurements at different saturations. Similar to Figure 5, a range of 5% error in saturation is included in the predictions. The results in Figure 6 convincingly demonstrate the capability of the proposed failure criterion in predicting the strength of partially saturated frozen soils at different degrees of saturation.

The accuracy of the model in predicting strength of unsaturated frozen soils is particularly impressive recalling that no retrospective calibration is carried out for the predictions in Figure 5 and 6. Nevertheless, it should be mentioned that the model has been developed and verified for non-cohesive soils such as sand and silt whose microscopic fabric is consistent with assumptions of the proposed model.
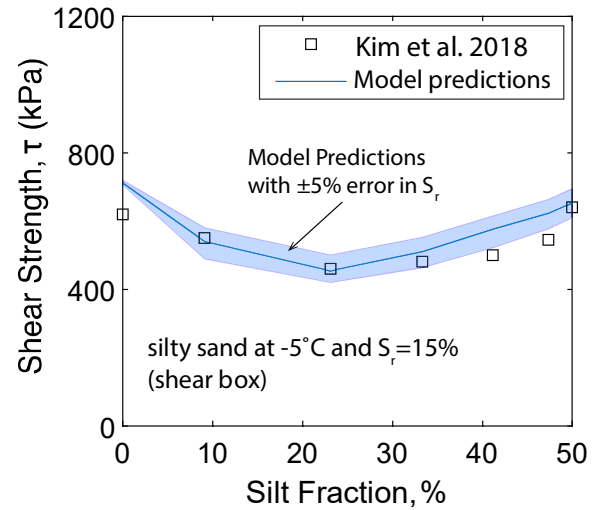

Figure 5. Comparing model predictions with the shear box experiments by Kim et al. (2018).
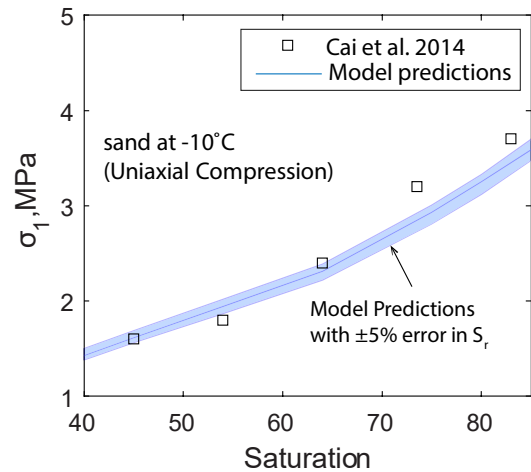

Figure 6. Comparing model predictions with the uniaxial compression tests by Cai et al. (2014) on saline frozen sand.

5   STRENGTH DEGRADATION DUE TO THAWING

Assessing the geotechnical hazards caused by warming climate in Northern regions depends crucially on a reliable estimate of strength degradation in frozen soils upon thawing. The failure criterion developed in this study is built on an analogy between the strength of the unsaturated soil at frozen and unfrozen states and as such, it can be readily used to estimate the strength degradation during thawing. In this case, the strength of the unsaturated soil at the unfrozen state is estimated by the commonly used Bishop's equation for effective stress materials (Bishop 1959) which takes the following form

$$\sigma' = (\sigma - u_a) + \chi (u_a - u_w) \qquad [8]$$

where $(\sigma - u_a)$ is the net stress at failure, and χ is the Bishop's effective stress parameter which is assumed to be the same as saturation ratio as suggested in the literature (Bishop 1959, Lu and Likos 2004).

The degradation of strength is explored here for the Ottawa sand with cohesion and friction angle of $c = 0$ and $\varphi = 30°$ (Mirshekari and Ghayoomi 2017). The WRC for the Ottawa sand is imported from Murthy et al. (2007). Figure 7 shows the comparison between the strength of the frozen and unfrozen states of unsaturated Ottawa sand at matric suction of $16\ kPa$.

As expected, due to its enhanced cohesion, the frozen soil exhibits significantly higher shear strength at lower normal stresses. Therefore, thawing is expected to induce a more drastic degradation in strength in these stress ranges. Curiously, the higher friction of the unfrozen soils causes the two envelopes to cross at higher normal stresses which indicates that below a certain limit, the unfrozen soil is expected to be stronger than the frozen. Assuming a typical unit weight of $18\ kN/m^3$, the intersect of the two envelopes occurs at a depth of approximately $30\ m$. Similar comparison but for the saturated soils has been offered by Zhou & Meschke (2018).

6   CONCLUSION

We presented in this study a micromechanical formulation that derives a failure criterion for frozen sandy and silty soils at partially saturated states. The microstructure of the soil is represented by spheres bonded to each other by cohesive ice bridges. The geometry of these ice bridges is related to those of the capillary liquid bridges at unfrozen state. This led to a Mohr-coulomb type failure criterion that depends on basic physics such as intrinsic strength of ice, contact fabric, particle size, and void ratio. Being based on fundamental properties of ice, the model indirectly takes into account strain rate and temperature dependency of the global strength, as visualized in a parametric study.

The model predictions are verified against two experimental datasets and the results indicate that the model can successfully predict the strength of frozen soils and how it varies with parameters such as saturation and fine content. The accuracy of the model in predicting the experimental observations is particularly remarkable because no retrospective calibration is carried out for enforcing the predictions to match the experimental results.

Finally, the model is used to estimate the degradation of strength in partially frozen sands upon thawing. The results show that while at loser confining stresses the frozen soil is stronger than the unfrozen soil, the failure envelopes cross at higher confining stresses due to higher friction of the unfrozen soils.
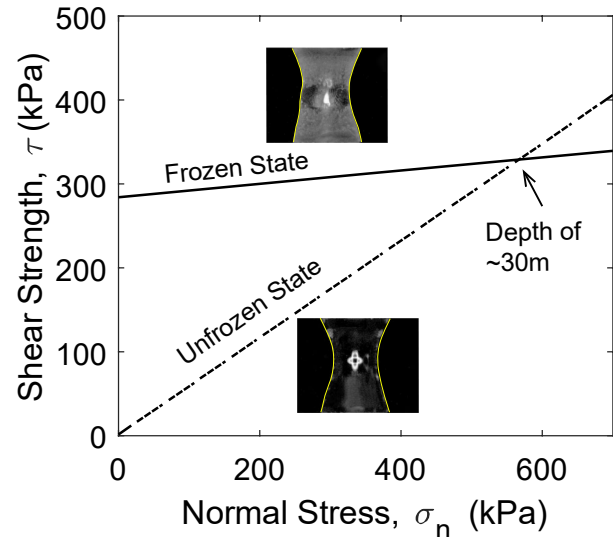

Figure 7. Mohr-Coulomb failure envelope for partially saturated Ottawa sand at frozen and unfrozen states. Inset images are adopted from Huang & Zhou (2020).

7   ACKNOWLEDGEMENTS

8   REFERENCES

Aksenov, V., Gevorkyan, S., and Doroshin, V. 2018. Dependence of Strength and Physical Properties of Frozen Sands on Moisture Content. Soil Mechanics & Foundation Engineering, **54**(6).

Arenson, L.U., and Springman, S.M. 2005. Mathematical descriptions for the behaviour of ice-rich frozen soils at temperatures close to 0 C. Canadian Geotechnical Journal, **42**(2): 431–442. NRC Research Press Ottawa, Canada.

Baker, T.H.W. 1979. Strain rate effect on the compressive strength of frozen sand. Engineering Geology, **13**(1–4): 223–231. Elsevier.

Bishop, A.W. 1959. The principle of effective stress. Teknisk ukeblad, **39**: 859–863.

Bourbonnais, J., and Ladanyi, B. 1985. The mechanical behaviour of frozen sand down to cryogenic temperatures. *In* International symposium on ground freezing. 4. pp. 235–244.

Bragg, R.A., and Andersland, O. 1981. Strain rate, temperature, and sample size effects on compression and tensile properties of frozen sand. Engineering Geology, **18**(1–4): 35–46. Elsevier.

Cai, Z., Wu, Z., Huang, Y., and others. 2014. Influence of water and salt contents on strength of frozen soils. Chinese Journal of Geotechnical Engineering, **36**(9): 1580–1586.

Chamberlain, E., Groves, C., and Perham, R. 1972. The mechanical behaviour of frozen earth materials under high pressure triaxial test conditions. Geotechnique, **22**(3): 469–483. Thomas Telford Ltd.

Fish, A.M., Zaretsky, Y.K., and others. 1997. Ice strength as a function of hydrostatic pressure and temperature. Cold Regions Research and Engineering Laboratory (US).

Huang, W., and Zhou, X. 2020. Freezing of axisymmetric liquid bridges. Physical Review Fluids, **5**(10): 103601. APS.

Kim, S.Y., Hong, W.-T., and Lee, J.-S. 2018. Silt fraction effects of frozen soils on frozen water content, strength, and stiffness. Construction and Building Materials, **183**: 565–577. Elsevier.

Konrad, J.-M. 1989. Physical processes during freeze-thaw cycles in clayey silts. Cold Regions Science and Technology, **16**(3): 291–303. Elsevier.

Ladanyi, B. 1972. An engineering theory of creep of frozen soils. Canadian Geotechnical Journal, **9**(1): 63–80. NRC Research Press Ottawa, Canada.

Liu, Z., Cai, G., Kong, X., Li, J., and Zhao, C. 2020. A thermodynamics-based mathematical model for the frost heave of unsaturated freezing soils. Cold Regions Science and Technology, **178**: 103125. Elsevier.

Lu, N., and Likos, W.J. 2004. Unsaturated Soil Mechanics. Wiley, New York.

Mirshekari, M., and Ghayoomi, M. 2017. Centrifuge tests to assess seismic site response of partially saturated sand layers. Soil Dynamics and Earthquake Engineering, **94**: 254–265. Elsevier.

Morgenstern, N., and Anderson, D.M. 1973. Physics, chemistry, and mechanics of frozen ground: a review. *In* Permafrost: North American Contribution [to The] Second International Conference. National Academies. p. 257.

Murthy, T., Loukidis, D., Carraro, J., Prezzi, M., and Salgado, R. 2007. Undrained monotonic response of clean and silty sands. Géotechnique, **57**(3): 273–288. Thomas Telford Ltd.

Pouragha, M., Eghbalian, M., and Wan, R. 2020. Micromechanical correlation between elasticity and strength characteristics of anisotropic rocks. International Journal of Rock Mechanics and Mining Sciences, **125**: 104154. Elsevier.

Pouragha, M., Eghbalian, M., Wan, R., and Wong, T. 2021. Derivation of soil water retention curve incorporating electrochemical effects. Acta Geotechnica, **16**(4): 1147–1160. Springer.

Pouragha, M., Wan, R., Duriez, J., and Sultan, N.H. 2018. Statistical analysis of stress transmission in wet granular materials. International Journal for Numerical and Analytical Methods in Geomechanics, **42**(16): 1935–1956. Wiley Online Library.

Pouragha, M., Wan, R., and Eghbalian, M. 2019. Critical plane analysis for interpreting experimental results on anisotropic rocks. Acta Geotechnica, **14**(4): 1215–1225. Springer.

Smith, T., and Schulson, E. 1994. Brittle compressive failure of salt-water columnar ice under biaxial loading. Journal of Glaciology, **40**(135): 265–276. Cambridge University Press.

Wan, R., Khosravani, S., and Pouragha, M. 2014. Micromechanical analysis of force transport in wet granular soils. Vadose Zone Journal, **13**(5): vzj2013-06. The Soil Science Society of America, Inc.

Wang, P., Liu, E., and Zhi, B. 2021. An elastic-plastic model for frozen soil from micro to macro scale. Applied Mathematical Modelling, **91**: 125–148. Elsevier.

Wang, P., Liu, E., Zhi, B., and Song, B. 2020. A macro–micro viscoelastic-plastic constitutive model for saturated frozen soil. Mechanics of Materials, **147**: 103411. Elsevier.

Yamamoto, Y., and Springman, S.M. 2014. Axial compression stress path tests on artificial frozen soil samples in a triaxial device at temperatures just below 0 C. Canadian Geotechnical Journal, **51**(10): 1178–1195. NRC Research Press.

Zhou, M.-M., and Meschke, G. 2018. A multiscale homogenization model for strength predictions of fully and partially frozen soils. Acta Geotechnica, **13**(1): 175–193. Springer.